How to cite: *Angew. Chem. Int. Ed.* **2025**, *64*, e202423912
doi.org/10.1002/anie.202423912

Supramolecular Chemistry

Orderly Arranged Cubic Quantum Dots along Supramolecular Templates of Naphthalenediimide Aggregates

Amrutha Manoj Lena, Mitsuaki Yamauchi, Hideyuki Murakami, Naoki Kubo, Sadahiro Masuo, Kyohei Matsuo, Hironobu Hayashi, Naoki Aratani,* and Hiroko Yamada**

Abstract: Precise control of assembled structures of quantum dots (QDs) is crucial for realizing the desired photophysical properties, but this remains challenging. Especially, the one-dimensional (1D) control is rare due to the nearly isotropic nature of QDs. Herein, we propose a novel strategy for controlling the 1D-arrangement range of cubic perovskite QDs in solution based on the morphological modification of a supramolecular polymer (SP) template. The original template with a short and tangled fibrous structure is prepared in a low-polarity solvent mixture via self-assembly of a naphthalenediimide-functionalized cholesterol derivative with an adhesion group for QDs. Mixing this template with QDs leads to the co-aggregation into short-range 1D-arrays of QDs on the templates. Notably, subsequent heating and cooling of the co-aggregate solution forms longer-range 1D-arrays of QDs with lateral growth, where arranged QDs are sandwiched between reconstructed SP templates. Furthermore, the longer-range 1D-array of QDs is achieved via an alternative route involving the pre-organization of templates into longer and dispersed fibers by heating and cooling of the original template, succeeded by co-assembly with QDs. Finally, we reveal continuous fluorescence resonance energy transfer between 1D-arranged QDs by an in-depth analysis of the photoluminescence decay curves.

Introduction

Semiconductor nanocrystals, called quantum dots (QDs), are regarded as outstanding photoluminescent (PL) nanomaterials that have potential for a wide range of applications in interdisciplinary research areas, such as optoelectronics,[1–2] bioimaging,[3–4] catalysis,[5–6] displays,[7–9] and so on. Among QDs, perovskite QDs, specifically cesium lead halide-based QDs ($CsPbX_3$, X = Cl, Br, I), have gained prominence in the field of luminescent materials. They offer high luminous efficiency, narrow PL linewidths that give high color purity, tunable PL wavelengths (by manipulating the halide composition), and high photodurability.[10–12] Recent researches have focused on the ordered spatial integration of individual QDs. This is because their assembly affords advanced photophysical properties, such as long-range exciton diffusion,[13–14] collective PL (superfluorescence),[15–16] and quantum resonance,[17–18] that cannot be realized in single and randomly assembled states. These properties are attributed to the ordered array structures of QDs, which exhibit efficient exciton transfer and/or electron- and exciton-coupling interactions. In previous studies, QD array structures have been constructed mainly by solvent-evaporation-induced self-assembly on a substrate, leading to two-dimensional (2D)- and three-dimensional (3D)-ordered assemblies of QDs, such as superlattices.[15] In contrast to these structures, one-dimensional (1D) ordered assemblies of QDs do not form spontaneously because of the difficulty in the anisotropic arrangement of isotropic QDs.

Several research groups,[19–22] including ours[23–26] have reported template methods for forming anisotropic 1D-arrays of spherical QDs using supramolecular assemblies of polymers, small organic molecules, and inorganic nanostructures. The template methods have been also utilized for the arrangement of metal nanoparticles.[27–28] Among these templates, supramolecular assembly templates can accurately control the location of the QDs based on the template structure. Recently, we have succeeded in the 1D-array formation of spherical CdSe and CdSe/ZnS QDs using a supramolecular polymer (SP) template composed of a cholesterol derivative with hydrogen bonding moieties and

[*] A. Manoj Lena, Prof. Dr. N. Aratani
Division of Materials Science
Nara Institute of Science and Technology (NAIST)
8916-5 Takayama-cho, Ikoma, Nara 630-0192 (Japan)
E-mail: aratani@ms.naist.jp

Dr. M. Yamauchi, H. Murakami, Dr. K. Matsuo, Prof. Dr. H. Yamada
Institute for Chemical Research
Kyoto University
Gokasho, Uji, Kyoto 611-0011 (Japan)
E-mail: yamauchi.mitsuaki.4u@kyoto-u.ac.jp
hyamada@scl.kyoto-u.ac.jp

N. Kubo, Prof. Dr. S. Masuo
Department of Applied Chemistry for Environment
Kwansei Gakuin University
1 Gakuen, Uegahara, Sanda, Hyogo 669-1330 (Japan)

Dr. H. Hayashi
Center for Basic Research on Materials
National Institute for Materials Science (NIMS)
1-2-1 Sengen, Tsukuba, Ibaraki 305-0047 (Japan)

an adhesion moiety (carboxyl group) for QDs (Figure 1a).[26] However, the rational methodology to control the arrangement range of QDs using SP templates has not yet been established. In addition, the 1D-arrangement of cubic QDs remains challenging.[29] As a rare example, Pan et al. reported the 1D-array of cubic $CsPbBr_3$ QDs using a pod-shaped $PdSO_4$ scaffold.[30] If this methodology using SP templates is established, more effective interactions between cubic QDs can occur via their flat surfaces.

Herein, we report a new strategy to control the 1D-array structures of cubic $CsPbBr_3$ QDs, achieving short- and longer-range organization through fine-tuning of the SP template morphology (Figures 1c,d). This template consists of chiral self-assemblies of naphthalenediimide (NDI)-functionalized cholesterol derivative **1** (Figure 1b), possessing a pyridyl group as adhesion moiety for QDs. Figure 1d summarizes the co-aggregation routes into short- and longer-range 1D-array of QDs based on transmission electron microscopy (TEM) observation. Upon adding poor solvent to the monomeric solution, **1** self-assembled into short and tangled fibrils (template A). Subsequently, mixing them with QDs resulted in short-range 1D-arrays of QDs via the adhesion of QDs on the templates. Notably, upon consecutive heating and cooling of the co-aggregate solution (thermal treatment), longer-range 1D-arrays of QDs with lateral growth, in which they are sandwiched between the reconstructed SP template, were formed. In addition, we found that the longer-range 1D-array of QDs could be formed also via an alternative co-aggregation route. In this route, longer and dispersed fibrils of **1** (template B) were pre-organized by thermal treatment of the template A in solution and then co-assembled with QDs to form the longer-range 1D-array. An in-depth analysis of the PL decay curves revealed continuous efficient fluorescence resonance energy transfer (FRET) among the 1D-arranged QDs. To the best of our knowledge, this study is the first example of managing the 1D-array range of cubic QDs utilizing SP templates.

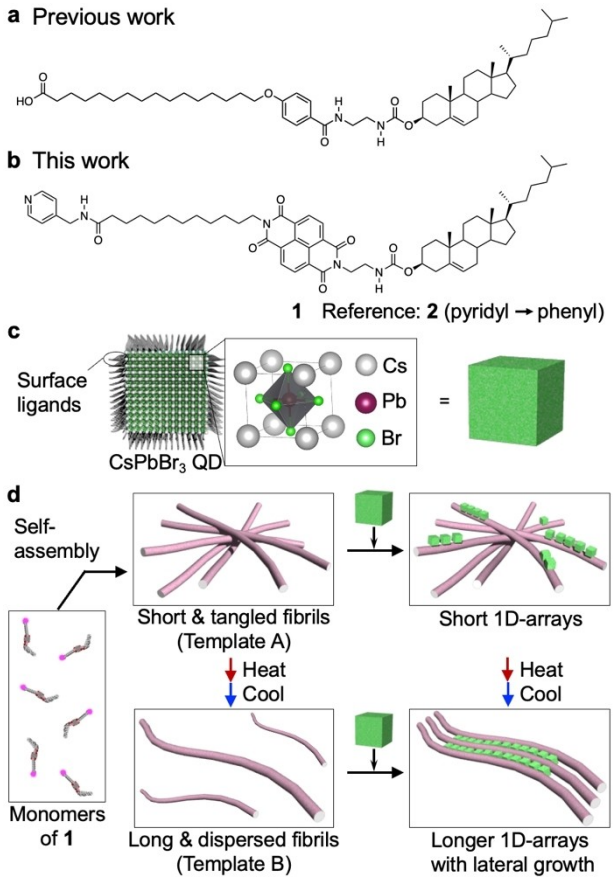

Figure 1. Molecular structures of (a) the previous compound and (b) **1** and **2**. (c) Chemical structure of $CsPbBr_3$ QD. (d) Schematic illustration of the 1D-array formation of QDs on different templates of **1**.

Results and Discussion

In this work, the adhesion between the SP template and QDs was essential for the formation of arranged QDs. In the previous work, the use of carboxyl group as adhesion moiety for QDs (Figure 1a)[26] can form unfavorable hydrogen-bonded dimers without exposed adhesion sites for QDs. Therefore, we newly designed a cholesterol derivative **1** with a pyridyl group at the end of the molecule as a more appropriate adhesion moiety for QDs (Figure 1b). The cholesterol group was introduced at the other end as a soluble substituent in low-polarity solvents and a chiral moiety. Amide and carbamate groups were introduced to promote self-assembly by hydrogen bonds. NDI core unit,[31–33] a well-established class of molecules in supramolecular chemistry, is used as a π–π stacking moiety and their aggregation behaviors can be monitored by spectroscopic analyses. To confirm the adhesion effect of the pyridyl group indirectly, a reference compound **2** was synthesized by replacing the pyridyl group with a phenyl group (Figure 1b). **1** and **2** were synthesized in two steps using naphthalene-tetracarboxylic dianhydride as the starting reagent. The synthetic schemes and characterization data of **1** and **2** using ^{1}H- and ^{13}C-nuclear magnetic resonance (NMR) spectroscopy and high-resolution mass spectrometry (HRMS) are described in the Supporting Information (Schemes S1, S2, Figures S1–S9).

First, the absorption characteristics of **1** ($[\mathbf{1}] = 3.0\times10^{-4}$ M) were evaluated in chloroform ($CHCl_3$), where **1** was expected to exist predominantly in its monomeric state. The UV/Vis absorption spectrum demonstrated sharp peaks with absorption maxima at 380, 360, and 342 nm, corresponding to the π–π transitions of the NDI core in monomeric **1** (Figure 2a). To form aggregates of **1** in a low-polarity solvent mixture ($[\mathbf{1}] = 3.0\times10^{-4}$ M), a solution of **1** in $CHCl_3$/methylcyclohexane (MCH) (2:5, *v*/*v*) was prepared by adding 0.75 mL of MCH as a poor solvent into 0.30 mL of a $CHCl_3$ solution ($[\mathbf{1}] = 1.1\times10^{-3}$ M). The spectrum of the aggregates in solution showed broader peaks with a loss of vibronic structure and a slight increase in a new red-shifted absorption at approximately 400 nm (Figure 2a) indicating π–π stacking interactions between the NDI cores of the aggregate.[33] To obtain evidence of hydrogen bonding, we recorded the Fourier transform infrared (FT-IR) spectra of

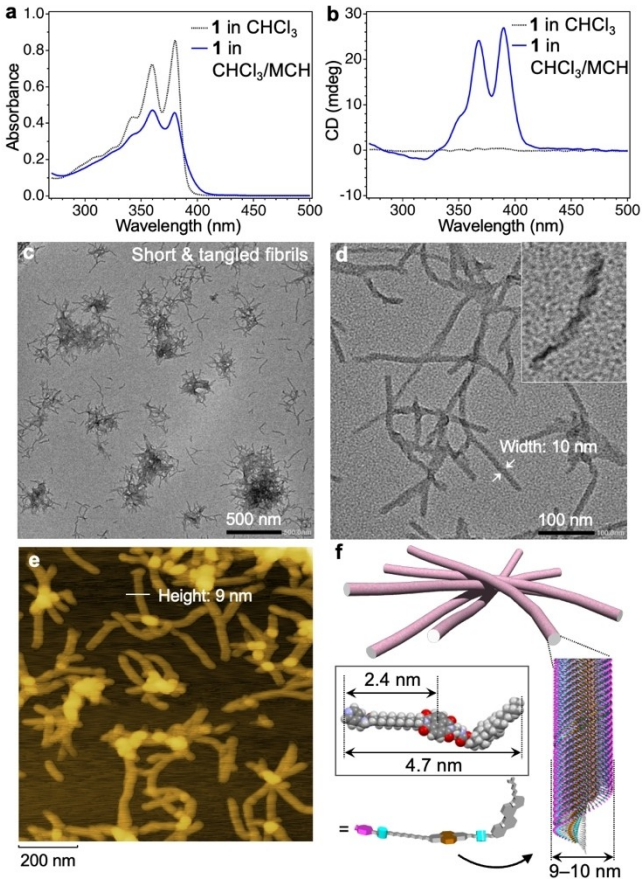

Figure 2. (a) UV/Vis absorption and (b) CD spectral changes of **1** ([**1**] = 3.0×10^{-4} M) in $CHCl_3$ and $CHCl_3$/MCH (2:5, *v*/*v*). (c, d) TEM and (e) AFM images of the nanofibrils of **1**. Inset in (d) is a magnified image of helical structure. (f) Schematic illustration of a possible aggregate structure of **1**.

the same solutions (monomeric **1** in $CHCl_3$ and aggregated **1** in $CHCl_3$:MCH (2:5, *v*/*v*)). The FT-IR spectra are shown in Figure S10a. Monomeric **1** showed a free N–H peak at 3452 cm^{-1}, while aggregated **1** showed the emergence of extra broad N–H peaks in the shorter wavenumber region at 3345 and 3262 cm^{-1}. This result indicates the existence of two types of hydrogen bonding modes for amide and carbamate groups, attributed to different hydrogen bond strengths.

The supramolecular chirality of aggregated **1** based on the chiral exciton coupling between the NDI cores, was determined from the variations in circular dichroism (CD) signals from the monomeric to the aggregated state. Although the CD signal of monomeric **1** in $CHCl_3$ was negligible in the absorption region of the NDI cores because of the absence of chiral π–π stacking, aggregated **1** exhibited clear CD signals with two sharp positive peaks at 368 and 390 nm (Figure 2b). These CD signals suggest that **1** undergoes self-assembly via one-handed biased helical stacking.

The morphological features of the aggregates of **1** were assessed using TEM and atomic force microscopy (AFM). The TEM images reveal predominant formation of short and tangled nanofibrils (Figures 2c, d and S10b, c). The average width of a single nanofibril was measured to be ca. 10 nm. The AFM analysis revealed a height of ca. 9 nm (Figures 2e and S10d). Considering the above results, the nanofibril was expected to be a cylindrical structure with a diameter of 9–10 nm. This diameter is nearly twice the molecular length of **1** (4.7 nm) estimated from the energy-optimized structure using density functional theory (DFT) calculation (Figure 2f). Also, the nanofibril was expected to be formed via helical stacking of **1** based on the CD activity (Figure 2b). According to the results, we can exclude the possibility of a simpler single helical-growth with rotational stacks maintaining the molecular length, known as twisted ribbon[34] (Figure S10e). To be twice the molecular length, an offset stacking event should be involved in the helical-growth. Therefore, we conclude that multiple helical-growths into a tightly coiled ribbon or a tube-like structure[34] occurred as the major self-aggregation process rather than a single helical-growth (Figures 2f and S10e). Occasionally, the helical nanostructures with pitch were observed as a screwed tube structure (Figure 2d inset), which supported the helical-growth mechanism.

Similarly, we investigated the self-assembly behavior of the reference compound **2**. In $CHCl_3$/MCH (2:5, *v*/*v*), in which **1** self-assembled, **2** existed as monomers, as confirmed by the sharp absorption peaks, absence of CD signals, and presence of an IR peak corresponding to free N–H moieties only (Figures S11a–c). This result indicates that **2** has a lower self-assembling ability than **1**, presumably because of the higher solubility of the phenyl group in **2** compared to the pyridyl group in **1** in the low-polarity solvent mixture. To induce the self-assembly of **2**, we attempted its aggregation at a higher ratio of MCH ($CHCl_3$:MCH = 1:7, *v*/*v*). The aggregate formation was confirmed by the broadening of absorption peaks, emergence of CD signals, and presence of new IR peaks corresponding to the hydrogen-bonded amide and carbamate groups (Figures S11a–c). Unlike **1**, **2** displayed increased light scattering effects on the absorbance towards longer wavelengths (Figure S11a), indicating the formation of larger aggregates. As predicted, larger tangled fibrils were confirmed using TEM (Figure S11d).

Cubic $CsPbBr_3$ QDs coated with surface ligands (oleic acid and oleylamine) were synthesized according to previously reported procedures (Figure 1c and Supporting Information).[10] TEM analysis of the QDs, spin-coated from the solution onto a grid, revealed the cube-shape of the QDs with an average edge-to-edge length of 7.8 ± 1.0 nm (Figures S12a, b). The TEM images showed assembled structures of the QDs formed by drying their dispersed solution on the substrate. The molar concentration of QD solution, assuming a single QD as a molecule, was estimated using an absorption spectrum in solution according to the reported method.[35]

Previously, the interaction between nitrogen atoms of the pyridyl group and Pb atoms of formamidinium (or methylammonium) lead halide perovskite crystals has been reported in the solid state.[36–37] However, the dynamic interaction in solution has not been revealed. To obtain insight into the adhesion of **1** to QD, we compared the ^1H

NMR spectra of **1**, QD, and their mixture ([**1**]:[QD] = 100:1) in [D_8]toluene (Figure S13). Upon mixing **1** with QD, the original proton signal of the pyridyl group of **1** showed a slight shift with a signal broadening, while the proton signals of the NDI and cholesterol moieties did not change. This implies the adhesion of the pyridyl moiety on the QD surface.

The short and tangled nanofibrils of **1** can serve as SP templates (referred to as template A) because their surfaces contain pyridyl groups as adsorption sites for QDs. Thus, the arrangement of QDs using the SP template was attempted by mixing the fibrous aggregate of **1** and QDs in solution. First, we prepared a QD solution ([QD] = ca. 1×10^{-7} M) in $CHCl_3$/MCH (2:5, *v*/*v*) and dried it to be a film under argon flow. Subsequently, it was mixed with an aggregate solution of **1** ($CHCl_3$:MCH = 2:5, *v*/*v*, [**1**] = 3.0×10^{-4} M). The molar ratio of **1**:QD in the mixture was maintained at 3000:1. To confirm the adhesion of the QDs onto the template, TEM observation of the co-aggregates was carried out (Figures 3a–d). The images revealed the adhesion of the QDs to the tangled fibrous template A, in which 1D-arrangement of several QDs (short-range 1D-array) was observed along the surfaces of the templates (Figure 3e). In addition, we can infer that the adsorption of QDs on the template was highly favorable, as no free or self-assembled QDs were observed on other areas (Figures S14a,b). In the adhesion process, the exposed pyridyl groups on the template interchange with the original surface ligands, oleic acid and oleylamine, of QDs, via a ligand-exchange reaction[38] and/or contact to a site without ligands or a halide vacancy on the surface.[39]

In contrast, the TEM images of a mixture of self-assembled **2** and QDs revealed mainly isolated regions of **2** and QDs, namely phase separation via narcissistic self-sorting (Figure S15a). Unlike the combination of **1** and QD, self-assembled QDs formed by the evaporation of solvents on the substrate were also observed (Figure S15b). Thus, we indirectly conclude that the pyridyl groups on the SP template of **1** serve as effective adhesion moieties for QDs.

Next, we investigated the photophysical interactions between the SP template A of **1** and QDs. The UV/Vis absorption spectrum after mixing them was nearly consistent with the sum of their individual spectra (Figure 4a). This result excludes electronic interactions between QD and **1** in the ground state. In addition, no clear CD spectral changes were observed after mixing (Figure 4b), indicating that the adhesion of QDs did not disrupt the chiral stacking of **1**. In contrast, the PL spectra of QDs under an irradiation of 470 nm, at which only QDs are excited, showed a decrease in the PL intensity upon mixing with template A (Figure 4a). This result suggests an increase in other nonradiative processes via interactions between QD and **1** and/or arranged QDs in the excited state.

To investigate the thermal reversibility of the 1D-arranged structure of QDs along the SP template, we prepared an original solution ([**1**]:[QD] = 3000:1, [**1**] = 3.0×10^{-4} M) by mixing an aggregate solution of **1** ($CHCl_3$:MCH = 2:5, *v*/*v*, [**1**] = 3.0×10^{-4} M) and a film prepared by drying a QD solution ([QD] = ca. 1×10^{-7} M). After heating the original solution at 90 °C and subsequent cooling to 20 °C, the arrangement level of QDs on the template changed (Figures 5a–c and S16). The TEM images revealed the formation of not only short-range 1D-arrays, but also longer-range ordered 1D-arrays of QDs, compared to the original arrangement structures before heating and cooling

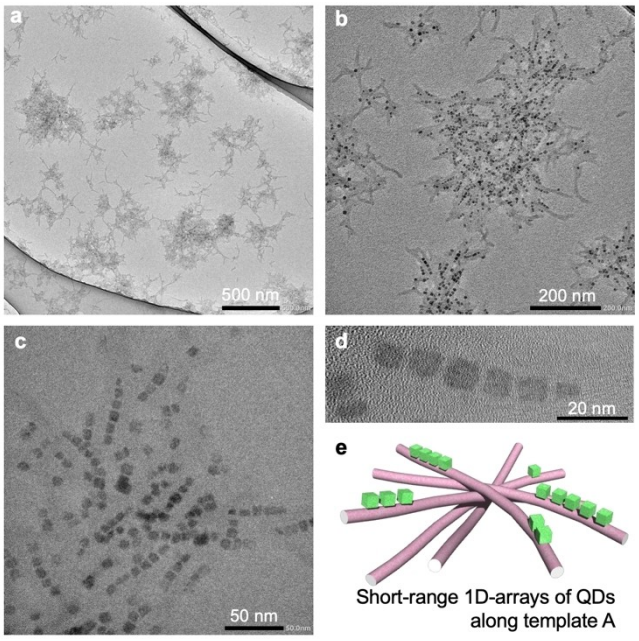

Figure 3. (a) TEM image and (b–d) the magnified images of 1D-arranged QDs along the SP template A of **1**. (e) Schematic illustration of the co-aggregate model structure.

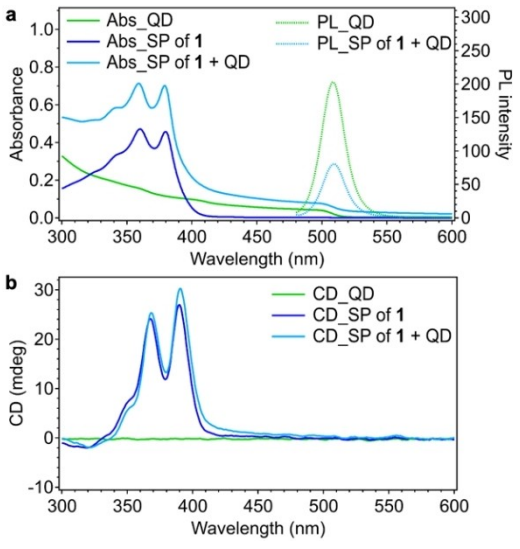

Figure 4. (a) UV/Vis absorption, PL, and (b) CD spectra of the dispersed QDs ([QD] = ca. 1×10^{-7} M), the SP template A of **1** ([**1**] = 3.0×10^{-4} M), and co-aggregates of the SP template A of **1** and QD ([**1**]:[QD] = 3000:1; [**1**] = 3.0×10^{-4} M) in $CHCl_3$/MCH (2:5, *v*/*v*). The excitation wavelength of PL spectra was 470 nm.

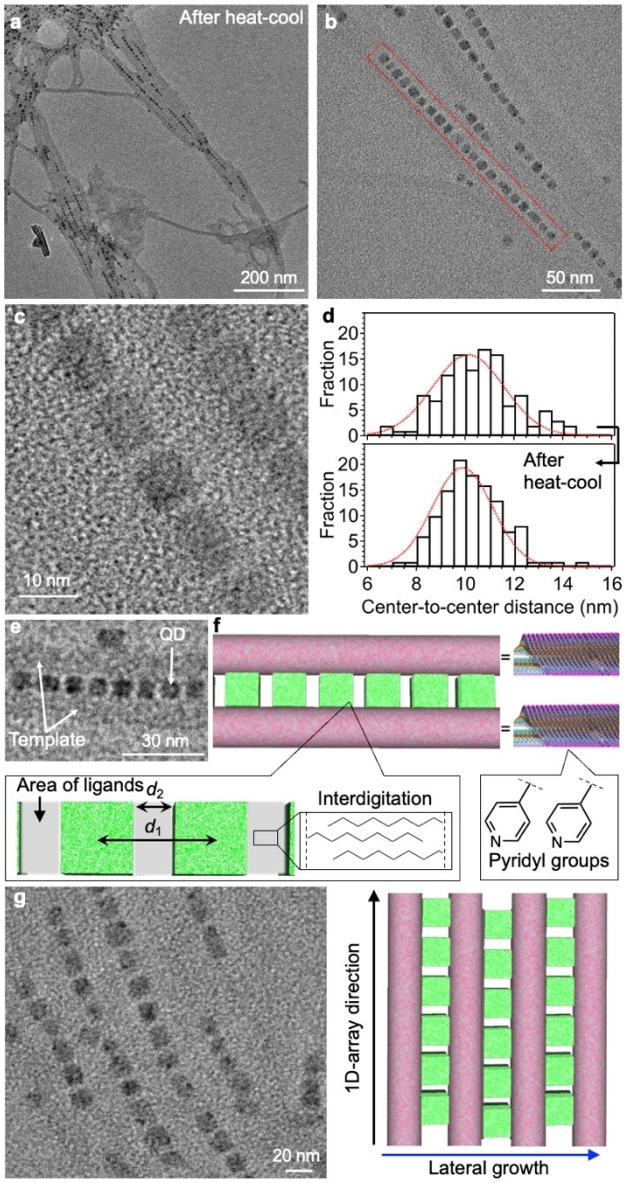

Figure 5. (a–c) TEM images of longer-range 1D-arranged QDs on templates of **1** after heat-cool treatment. (d) Histogram of the center-to-center distance between 1D-arranged QDs. Top and bottom histograms correspond to the short- and longer-range 1D-arranged QDs, respectively. (e) TEM image of 1D-arranged QDs sandwiched between the templates, obtained under a different focus mode. (f) Schematic illustration of the 1D-arranged nanostructure of QDs, in which d_1 and d_2 are the center-to-center and edge-to-edge distance, respectively. (g) TEM image of 1D-arranged QDs with lateral growth and the model structure.

(Figures 3a–c). The longest 1D-array consisted of 21 QDs with length ~200 nm (Figure 5b). In these TEM images, longer SPs of **1** were observed as templates for the longer-range 1D-array of QDs, suggesting that the template structure was re-constructed via the heat-cool treatment. Notably, the 1D-arranged QDs were found to be sandwiched between the re-constructed SP templates (Figure 5e). The model co-aggregate structure is shown in Figure 5f.

The QDs were orderly arranged in 1D-array orienting their flat facets in the same direction, namely, face-to-face overlapping configuration (Figures 5c, f). To compare this longer-range and the original short-range 1D-arrays (before heat-cool), we measured the center-to-center distance (d_1) between the arranged QDs for more than 100 array points. The histograms are shown in Figure 5d. The average value of d_1 for the longer-range 1D-array was 10.3 ± 1.3 nm. This standard deviation was derived from the size distribution of QDs (7.8 ± 1.0 nm). For the original 1D-array, the average value of d_1 was 10.5 ± 1.6 nm, which was slightly larger than that of the longer-range 1D-array. This result implies that the heat-cool treatment induces not only the formation of a longer-range 1D-array of QDs, but also a more uniform face-to-face overlapping configuration. Furthermore, the edge-to-edge distance (d_2) between the 1D-arranged QDs was estimated to be ~2 nm from the TEM images. Considering that this distance is less than twice the lengths of surface ligands oleic acid and oleylamine, interdigitation between the surface ligands occurs via van der Waals interactions (Figure 5f). This interdigitation can lead to face-to-face overlapping of the arranged QDs.

Notably, we found a lateral growth of 1D-arranged QDs perpendicular to the 1D-array direction by TEM imaging (Figures 5g and S16). This means the formation of a multilayer sandwich structure with repeated alternate arrangement of 1D-array of QDs and SP of **1**. The lateral interaction is presumably because the SP template has an adhesion ability on both sides, which is derived from the helical morphology.

Next, we increased the concentration of QDs in the co-aggregate to approximately 3×10^{-7} M ([**1**]:[QD] = 3000:3) and performed heat-cool treatment. TEM images displayed more densely adsorbed QDs with long-range 1D-array structures along the SP template (Figures S17a–c). One of the longest 1D-arrays of QDs measured ~400 nm. Free QDs that were not adsorbed on the template were also observed, suggesting that this concentration of QDs was over the capacity of the templates.

We then investigated the thermal effect on the change of 1D-array structures of QDs along the templates of **1** by further heat-cool treatments. However, the TEM images showed only a few 1D-array structures after twice heat-cool treatment of the solution. In addition, fibrous templates without QDs and largely fused QDs were mainly observed (Figures S18a–c). This is probably due to the thermally induced agglomeration or decomposition of QDs.

Here, we discuss the mechanism for the formation of a longer-range 1D-array of QDs by the heat-cool process. We measured the CD spectrum of the co-aggregate ([**1**]:[QD] = 3000:1, [**1**] = 3.0×10^{-4} M) at 90 °C to investigate the change in the stacking nature of **1** upon heating. The CD signals of the co-aggregates decreased but did not completely disappear (Figure S19a), indicating the presence of monomers and aggregates of **1** at 90 °C. In contrast, the self-aggregates of **1** showed a more pronounced decrease in CD signals upon heating to 90 °C (Figure S19b). The higher thermal stability of the co-aggregates was probably due to the adsorption of QDs onto the template of **1**. This hot solution

was directly spin-coated onto a grid, and the samples were observed using TEM. The images revealed that the short-range 1D-array of QDs on the template of **1** persisted even at high temperatures (Figures S19c,d). Additionally, short fibers of **1**, randomly assembled QDs, and free QDs were observed. After cooling to 20 °C, the CD signals recovered due to the reassembly of **1** (Figure S19a). Consequently, cooling led to the formation of longer-range 1D-arrays of QDs (Figure 5a). Based on these results, we propose the following reconstruction mechanism. At high temperatures, short-range 1D-arrays of QDs along the template of **1** coexist with the monomers of **1** and free QDs. During the cooling process, the monomers are consumed for the formation of more extended SP templates, and then free QDs are adsorbed and arranged along the re-constructed longer template.

From the above results, the formation of longer templates of **1** is a key factor to realize the longer-range 1D-array of QDs. We predicted that if a longer SP template can be prepared and then mixed with free QDs, a similar longer-range 1D-array of QDs can be formed. Therefore, we verified whether a longer fiber of **1** is formed in the absence of QDs by heat-cool treatment of the aggregate solution of **1** ($CHCl_3$:MCH (2:5, *v*/*v*), [**1**] = 3.0×10^{-4} M). As confirmed by TEM, longer and dispersed fibrils (referred to as template B), compared to the tangled short fibrils (template A) prepared by the original method, were formed upon cooling of a hot solution (~80 °C) (Figures 6a and S20). Subsequently, upon mixing them with QDs, longer-range 1D-arrangement of QDs along the longer template B was achieved as expected (Figures 6b,c and S21). The co-aggregates contained 1D-arranged QDs sandwiched between the templates and their lateral growth perpendicular to the 1D-array direction, similar to that obtained by the heat-cool treatment of the mixture (Figure 5a). This coaggregation method via pre-tuning of the template morphology was also effective at a lower concentration of **1** ([**1**] = 2.0×10^{-4} M), where longer-range 1D-arrays of QDs was obtained along the longer SP template (Figures 6d,e, and S22, S23). This result supports the usefulness and reproducibility of this method. As this method did not include the heating process of QDs, the QDs in the longer-range 1D-array structure did not suffer any thermal effects.

Finally, we discuss the interactions between an excited QD and templates of **1** or neighboring QDs. DFT calculations revealed the highest occupied molecular orbital (HOMO = −7.3 eV) and lowest unoccupied molecular orbital (LUMO = −3.8 eV) energy levels of the NDI core. Considering the conduction (−3.1 eV) and valence band (−5.6 eV) energy levels of $CsPbBr_3$ QDs from previously reported experimental values,[40] photoinduced electron transfer (eT) from the excited arranged QDs to NDI was anticipated (Figure 7a). Previously, eT from QD to monomeric NDI derivatives has been reported.[41] However, the possibility of eT in this case is low since the distance between the NDI core and edge of QD is not sufficiently short due to the presence of a long alkyl linkage between the pyridyl group and NDI core (2.4 nm, Figure 2f). Alternately, FRET between 1D-arranged QDs can occur

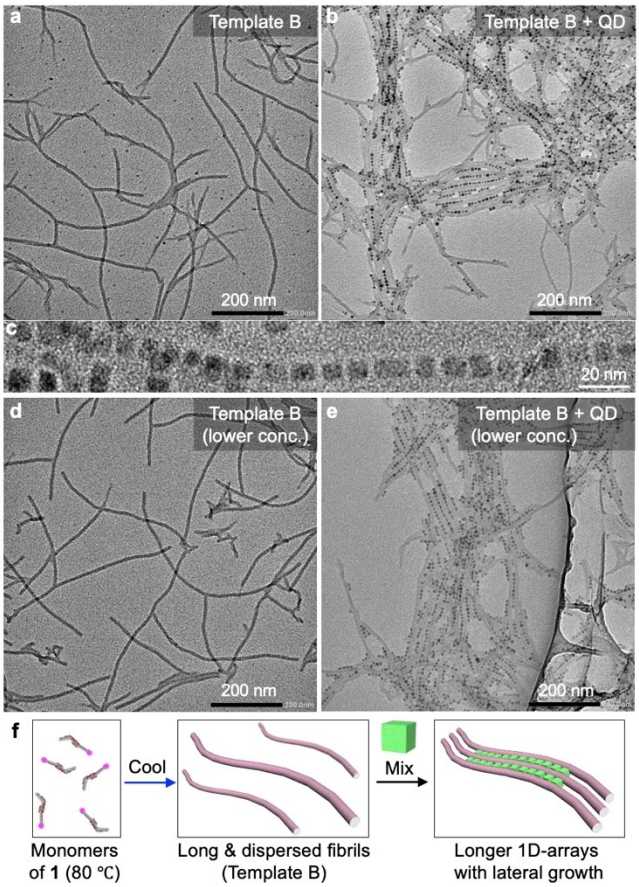

Figure 6. (a–c) TEM images of (a) SP template B ([**1**] = 3.0×10^{-4} M) (b) longer-range 1D-arranged QDs on the template, and (c) the magnified image. (d,e) TEM images of (d) SP template B at lower concentration of **1** ([**1**] = 2.0×10^{-4} M) and (e) longer-range 1D-arranged QDs on the template. (f) Schematic illustration of the co-aggregation process via template B.

through dipole–dipole interactions, as observed in the case of arranged spherical CdSe QDs.[25–26] The potential occurrence of FRET was supported by the sufficient spectral overlap between the PL and absorption spectra of the QDs (Figure S12c). This spectral overlap integral ($J(\lambda)$) value was estimated to be $1.06\times10^{17}\ M^{-1}(cm)^{-1}(nm)^4$ according to the method shown in Figure S12 caption, which is suitably large enough for FRET interactions. Förster radius (R_0), at which the FRET efficiency is 0.5, was estimated to be ca. 10 nm, which is comparable to d_1 (Figure 5d). In contrast, the possibility of FRET from QD to **1** was excluded due to the energy mismatch (Figure 4a). Therefore, it is expected that the arranged QDs along the SP templates of **1** predominately possess inter-QD FRET, rather than eT from QD to **1**, in the excited state of QDs (Figure 7b).

To evaluate the exciton dynamics of QDs among the co-aggregates in $CHCl_3$:MCH (2:5, *v*/*v*), we analyzed the PL decay curves of co-aggregates under an irradiation of 470 nm. The timing of measurements was set to 15 min after mixing SP with QDs to accurately compare the PL decay curves. Here, short-range 1D-array of QDs along template A (referred to as **Coagg-A**) and longer-range 1D-array of

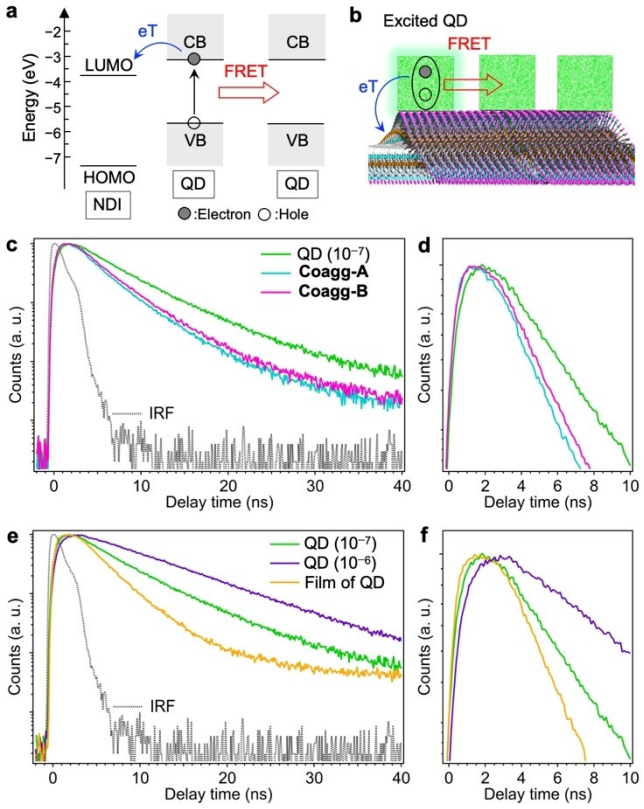

Figure 7. (a) Energy diagram of NDI and $CsPbBr_3$ QDs, where FRET and electron transfer (eT) upon excitation of QD are shown. (b) Schematic illustration of an exciton dynamics model among the arranged QDs on the SP template. (c) PL decay curves and (d) magnified curves of the dispersed QDs ([QD] = ca. 1×10^{-7} M) and co-aggregates of **1** and QD in $CHCl_3$/MCH (2 : 5, *v*/*v*). (e) PL decay curves and (f) magnified curves of dispersed QDs at different concentrations ([QD] = ca. 1×10^{-7} and 1×10^{-6} M) and the film of QD. The excitation wavelength was 470 nm.

QDs along template B (referred to as **Coagg-B**) were compared in the same conditions except for preparation routes ([**1**] : [QD] = 3000 : 1, [**1**] = 3.0×10^{-4} M). As a reference, the decay curve of dispersed QDs ([QD] = ca. 1×10^{-7} M) was measured. The PL decay curves are shown in Figure 7c. The curves were fitted using two exponential equations to estimate the PL lifetime (Figures S24a–c and Table S1). The results reveal a decrease in the average PL lifetime (τ) for QDs from 5.0 ns (τ_{QD}, dispersed QDs) to 3.1 ns ($\tau_{Coagg\text{-}A}$, **Coagg-A**) and 3.6 ns ($\tau_{Coagg\text{-}B}$, **Coagg-B**). Similar changes were reproducibly confirmed (Figures S25a–c and Table S2). The shortening of the PL lifetimes in **Coagg-A** and **Coagg-B** indicates the occurrence of nonradiative processes by the arrangement of QDs.

To unveil pure interactions between QDs, we measured PL spectrum and PL decay curve at 10 times higher concentration of QDs ([QD] = ca. 1×10^{-6} M). A red-shifted PL peak by 6 nm was observed compared to the original QD solution ([QD] = ca. 1×10^{-7} M) (Figure S26a). Unlike the case of original concentration, single component and longer PL lifetime (10.9 ns) was obtained with more delayed rise time (Figures 7e, f, S26b, and Table S3). These changes can be explained by multiple re-absorption and re-emission of photon, so-called photon recycling via radiative energy transfer (ET) process that is different mechanism from nonradiative FRET.[42–43] This photon recycling predominately occurs from smaller QD with larger band gap to larger QD with smaller band gap, resulting in the red-shifted PL. The red-shifted PL peak due to the re-absorption was also revealed in their superlattice.[44] Difference between the two ET mechanisms is whether there is a nonradiative process or not. Although FRET induces shortening of PL lifetime of donors, it is difficult to analyze PL lifetime components of donors because of the large PL overlap of donor and acceptor like this study's system. To obtain more accurate insight into interactions between QDs, we evaluated an aggregated QD film, in which QDs were located closely as mixture of randomly and orderly aggregated QDs. The film was prepared by drop-cast and drying of the QD solution ([QD] = ca. 1×10^{-7}) on a substrate. The PL decay curve afforded PL average lifetime ($\tau_{QD\text{-}film}$) of 3.6 ns (Figure S26c and Table S3), which was shorter than that of dispersed QDs (5.0 ns). As the change was induced by the aggregation of QDs, this shortening of the PL lifetimes was assignable to continuous FRET between aggregated QDs, so-called exciton diffusion. Due to the continuous FRET, the probability of exciton trapping by defects of QD can increase, resulting in the decrease of PL lifetimes.

Notably, the $\tau_{QD\text{-}film}$ value of QD films (3.6 ns), which is a suitable condition for continuous FRET, is consistent with the $\tau_{Coagg\text{-}B}$ value. Thus, we conclude that the longer-range 1D-array of QDs in the **Coagg-B** exhibits continuous FRET in solution, comparable to the QD films. In addition, **Coagg-A** exhibited a slightly shorter PL lifetime (3.1 ns) compared to that of the QD films (3.6 ns). This can be possibly explained due to the competitive eT from QD to SP in **Coagg-A** exhibiting FRET among short-range QD-arrays. When the contribution of eT increases, further shortening of PL lifetime can occur as observed. Especially, non-arranged (adsorbed) QDs on SP templates can show eT. Another explanation for the longer lifetime of **Coagg-B** than that of **Coagg-A** could be the efficient photon recycling across longer-range 1D-array of QDs, which enhances the PL lifetime.

Conclusion

In summary, we succeeded in controlling the short- and longer-range 1D-array structures of cubic perovskite QDs in solution by a new strategy of morphological tuning of SP template composed of NDI-functionalized cholesterol derivative with a pyridyl adhesion group. Upon mixing the dispersed QDs and SP templates with short and tangled fibrous structure in solution, the QDs self-arranged on the template into a short-range 1D-array, as revealed by TEM. A longer-range 1D-array of QDs was formed by using thermally tuned SP templates with longer and dispersed fibrous structure. Finally, we revealed continuous FRET between arranged QDs on the SP template by analyzing the PL decay curves. Our versatile strategy for efficiently self-

arranging QDs has the potential to contribute to the creation of long-range 1D-arranged superstructures of nanoparticles, enabling 1D anisotropic exciton and electron transfer among the assembled nanoparticles.

Supporting Information

Full details of synthesis, additional spectra, details of data collections are available in the Supporting Information.

Acknowledgements

This work was supported by Japan Society for the Promotion of Science (JSPS) KAKENHI Grant Numbers JP22K14556 to M.Y., JP24H01714 (Transformative Research Areas "Meso-Hierarchical Materials") to M.Y., JP24K01576 to H.H., JP23K26480 to N.A., JP20H00379 to H.Y., JP20H05833 (Transformative Research Areas "Dynamic Exciton") to H.Y., JP23K21106 to S.M., and JP23H04875 (Transformative Research Areas "Meso-Hierarchical Materials") to S.M.. A.M.L. thanks NAIST Granite program and NAIST University Fellowships for the Creation of Innovation in Science and Technology. This work was partially supported by NAIST-ARIM Program of MEXT, Japan. The TEM measurements were supported by the Advanced Research Infrastructure for Materials and Nanotechnology (JPMXP1222MS1029) of MEXT, Institute for Molecular Science, Instrument Center, Okazaki, Japan. We would like to thank Editage (www.editage.jp) for English language editing.

Conflict of Interest

The authors declare no conflict of interest.

Data Availability Statement

The data that support the findings of this study are available from the corresponding author upon reasonable request.

Keywords: perovskite quantum dot · supramolecular chemistry · self-assembly · naphthalenediimide · templated assembly

[1] S. Lee, M.-J. Choi, G. Sharma, M. Biondi, B. Chen, S.-W. Baek, A. M. Najarian, M. Vafaie, J. Wicks, L. K. Sagar, S. Hoogland, F. P. G. de Arquer, O. Voznyy, E. H. Sargent, *Nat. Commun.* **2020**, *11*, 4814.
[2] N. S. Peighambardoust, E. Sadeghi, U. Aydemir, *ACS Appl. Nano Mater.* **2022**, *5*, 14092–14132.
[3] W. R. Algar, K. Susumu, J. B. Delehanty, I. L. Medintz, *Anal. Chem.* **2011**, *83*, 8826–8837.
[4] P. Zrazhevskiy, X. Gao, *Nat. Commun.* **2013**, *4*, 1619.
[5] Y. Jiang, C. Wang, C. R. Rogers, M. S. Kodaimati, E. A. Weiss, *Nat. Chem.* **2019**, *11*, 1034–1040.
[6] Y. Li, Y. Gao, Z. Deng, Y. Cao, T. Wang, Y. Wang, C. Zhang, M. Yuan, W. Xie, *Nat. Commun.* **2023**, *14*, 4673.
[7] Y.-H. Suh, T. Kim, J. W. Choi, C.-L. Lee, J. Park, *ACS Appl. Nano Mater.* **2018**, *1*, 488–496.
[8] Y.-H. Ko, M. Jalalah, S.-J. Lee, J. G. Park, *Sci. Rep.* **2018**, *8*, 12881.
[9] D. Chen, D. Chen, X. Dai, Z. Zhang, J. Lin, Y. Deng, Y. Hao, C. Zhang, H. Zhu, F. Gao, Y. Jin, *Adv. Mater.* **2020**, *32*, e2006178.
[10] L. Protesescu, S. Yakunin, M. I. Bodnarchuk, F. Krieg, R. Caputo, C. H. Hendon, R. X. Yang, A. Walsh, M. V. Kovalenko, *Nano Lett.* **2015**, *15*, 3692–3696.
[11] G. Nedelcu, L. Protesescu, S. Yakunin, M. I. Bodnarchuk, M. J. Grotevent, M. V. Kovalenko, *Nano Lett.* **2015**, *15*, 5635–5640.
[12] H. Liu, Z. Liu, W. Xu, L. Yang, Y. Liu, D. Yao, D. Zhang, H. Zhang, B. Yang, *ACS Appl. Mater. Interfaces* **2019**, *11*, 14256–14265.
[13] M. Yang, P. Moroz, E. Miller, D. Porotnikov, J. Cassidy, C. Ellison, X. Medvedeva, A. Klinkova, M. Zamkov, *ACS Photonics* **2019**, *7*, 154–164.
[14] E. Penzo, A. Loiudice, E. S. Barnard, N. J. Borys, M. J. Jurow, M. Lorenzon, I. Rajzbaum, E. K. Wong, Y. Liu, A. M. Schwartzberg, S. Cabrini, S. Whitelam, R. Buonsanti, A. Weber-Bargioni, *ACS Nano* **2020**, *14*, 6999–7007.
[15] G. Rainò, M. A. Becker, M. I. Bodnarchuk, R. F. Mahrt, M. V. Kovalenko, T. Stöferle, *Nature* **2018**, *563*, 671–675.
[16] C. Zhou, Y. Zhong, H. Dong, W. Zheng, J. Tan, Q. Jie, A. Pan, L. Zhang, W. Xie, *Nat. Commun.* **2020**, *11*, 329.
[17] D. Kim, S. Tomita, K. Ohshiro, T. Watanabe, T. Sakai, I. Y. Chang, K. Hyeon-Deuk, *Nano Lett.* **2015**, *15*, 4343–4347.
[18] T. Lee, K. Enomoto, K. Ohshiro, D. Inoue, T. Kikitsu, K. Hyeon-Deuk, Y. J. Pu, D. Kim, *Nat. Commun.* **2020**, *11*, 5471.
[19] J. Sharma, Y. Ke, C. Lin, R. Chhabra, Q. Wang, J. Nangreave, Y. Liu, H. Yan, *Angew. Chem. Int. Ed.* **2008**, *47*, 5157–5159.
[20] Y.-J. Kim, C.-H. Cho, K. Paek, M. Jo, M.-K. Park, N.-E. Lee, Y.-J. Kim, B. J. Kim, E. Lee, *J. Am. Chem. Soc.* **2014**, *136*, 2767–2774.
[21] K. Enomoto, D. Inoue, Y.-J. Pu, *Adv. Funct. Mater.* **2019**, *29*, 1905175.
[22] B. Ni, C. Fu, S. Pan, L. He, Z. Lin, J. Peng, *Chem. Mater.* **2022**, *34*, 847–853.
[23] M. Yamauchi, S. Masuo, *Chem. Eur. J.* **2019**, *25*, 167–172.
[24] M. Yamauchi, S. Masuo, *Chem. Eur. J.* **2020**, *26*, 7176–7184.
[25] M. Yamauchi, S. Yamamoto, S. Masuo, *Angew. Chem. Int. Ed.* **2021**, *60*, 6473–6479.
[26] M. Yamauchi, K. Nakatsukasa, N. Kubo, H. Yamada, S. Masuo, *Angew. Chem. Int. Ed.* **2024**, *63*, e202314329.
[27] E. Zhu, S. Wang, X. Yan, M. Sobani, L. Ruan, C. Wang, Y. Liu, X. Duan, H. Heinz, Y. Huang, *J. Am. Chem. Soc.* **2019**, *141*, 1498–1505.
[28] F. Yang, X. Liu, Z. Yang, *Angew. Chem. Int. Ed.* **2021**, *60*, 14671–14678.
[29] Y. Ji, M. Wang, Z. Yang, S. Ji, H. Qiu, *J. Mater. Chem. C* **2019**, *7*, 8471–8476.
[30] A. Pan, M. Jurow, Y. Zhao, F. Qiu, Y. Liu, J. Yang, J. J. Urban, L. He, Y. Liu, *Nanoscale* **2017**, *9*, 17688–17693.
[31] M. R. Molla, S. Ghosh, *Chem. Eur. J.* **2012**, *18*, 9860–9869.
[32] S. M. Wagalgave, S. D. Padghan, M. D. Burud, M. A. Kobaisi, D. D. La, R. S. Bhosale, S. V. Bhosale, S. V. Bhosale, *Sci. Rep.* **2019**, *9*, 12825.
[33] D. S. Pal, H. Kar, S. Ghosh, *Chem. Eur. J.* **2016**, *22*, 16872–16877.
[34] T. Shimizu, M. Masuda, H. Minamikawa, *Chem. Rev.* **2005**, *105*, 1401–1443.

[35] J. Maes, L. Balcaen, E. Drijvers, Q. Zhao, J. De Roo, A. Vantomme, F. Vanhaecke, P. Geiregat, Z. Hens, *J. Phys. Chem. Lett.* **2018**, *9*, 3093–3097.
[36] T. Yang, C. Ma, W. Cai, S. Wang, Y. Wu, J. Feng, N. Wu, H. Li, W. Huang, Z. Ding, L. Gao, S. Liu, K. Zhao, *Joule* **2023**, *7*, 574–586.
[37] M. Dementyev, L. F. Jones, M. C. Brennan, T. A. Grusenmeyer, S. D. Waugaman, R. T. Mathers, R. J. Hickey, *RSC Appl. Polym.* **2024**, *2*, 857–869.
[38] S. R. Smock, T. J. Williams, R. L. Brutchey, *Angew. Chem. Int. Ed.* **2018**, *57*, 11711–11715.
[39] N. Fiuza-Maneiro, K. Sun, I. López-Fernández, S. Gómez-Graña, P. Müller-Buschbaum, L. Polavarapu, *ACS Energy Lett.* **2023**, *8*, 1152–1191.
[40] M. De Franco, M. Cirignano, T. Cavattoni, H. Bahmani Jalali, M. Prato, F. Di Stasio, *Opt. Mater.* **2022**, *13*, 100124.
[41] E. A. Morais, M. A. Lemes, N. R. S. Souza, A. S. Ito, E. L. Duarte, R. S. Silva, S. Brochsztain, J. A. Souza, *ACS Omega* **2024**, *9*, 22296–22304.
[42] M. van der Laan, C. de Weerd, L. Poirier, O. van de Water, D. Poonia, L. Gomez, S. Kinge, L. D. A. Siebbeles, A. F. Koenderink, T. Gregorkiewicz, P. Schall, *ACS Photonics* **2021**, *8*, 3201–3208.
[43] I.-H. Tsai, S. Narra, S. S. Bhosale, E. W.-G. Diau, *J. Phys. Chem. Lett.* **2023**, *14*, 2580–2587.
[44] D. Baranov, S. Toso, M. Imran, L. Manna, *J. Phys. Chem. Lett.* **2019**, *10*, 655–660.

Manuscript received: December 7, 2024
Accepted manuscript online: January 7, 2025
Version of record online: January 17, 2025